JGR Atmospheres

RESEARCH ARTICLE
10.1029/2018JD030120

Key Points:
- Residential sector emissions found to have a positive effective radiative forcing over China
- This radiative forcing is mainly due to the direct effect, with some contribution from the semidirect effect
- High sensitivity to uncertainty in fraction of black carbon emitted from the residential sector

Supporting Information:
- Supporting Information S1
- Data Set S1

Correspondence to:
S. Archer-Nicholls,
sa847@cam.ac.uk

Citation:
Archer-Nicholls, S., Lowe, D., Lacey, F., Kumar, R., Xiao, Q., Liu, Y., et al. (2019). Radiative effects of residential sector emissions in China: Sensitivity to uncertainty in black carbon emissions. *Journal of Geophysical Research: Atmospheres*, *124*, 5029–5044. https://doi.org/10.1029/2018JD030120

Received 4 DEC 2018
Accepted 25 MAR 2019
Accepted article online 3 APR 2019
Published online 2 MAY 2019

Author Contributions:
Conceptualization: E. Carter
Data curation: Q. Xiao, Y. Liu
Formal analysis: D. Lowe, R. Kumar
Methodology: D. Lowe
Project administration: E. Carter
Resources: Q. Xiao, Y. Liu
Software: D. Lowe, R. Kumar
Writing – review & editing: D. Lowe, R. Kumar, Y. Liu, E. Carter

Radiative Effects of Residential Sector Emissions in China: Sensitivity to Uncertainty in Black Carbon Emissions

S. Archer-Nicholls[1,2], D. Lowe[3], F. Lacey[1,3], R. Kumar[1], Q. Xiao[4], Y. Liu[4], E. Carter[5], J. Baumgartner[6], and C. Wiedinmyer[1,7]

[1]National Center for Atmospheric Research (NCAR), Boulder, CO, USA, [2]Now at Centre for Atmospheric Science, Department of Chemistry, University of Cambridge, Cambridge, UK, [3]Centre for Atmospheric Science, School of Earth, Atmospheric and Environmental Sciences, University of Manchester, Manchester, UK, [4]School of Environment, Tsinghua University, Beijing, China, [5]Walter Scott Jr. College of Engineering, Colorado State University, Fort Collins, CO, USA, [6]Institute for Health and Social Policy, Department of Epidemiology, Biostatistics and Occupational Health, McGill University, Montreal, Quebec, Canada, [7]Now at Cooperative Institute for Research in Environmental Science, University of Colorado Boulder, Boulder, CO, USA

Abstract Residential sector emissions of aerosols, primarily from solid fuels burned for cooking and heating purposes, are high in black carbon, a component that absorbs radiation efficiently across a wideband of wavelengths. Mitigation of residential sector emissions has been suggested as a method to rapidly reduce anthropogenic global warming. This study presents model results from a regional model with coupled chemistry, aerosols, and dynamics over an East Asian domain for January 2014 to investigate the radiative effects of residential sector emissions. Model results are evaluated against surface measurements of particulate matter and remote sensing products, comparing well but with a high aerosol optical depth bias over Sichuan and low single scattering albedo over many locations. We calculate effective radiative forcing of residential sector aerosols at the top of the atmosphere of +1.22 W/m^2 over Eastern China, +1.04 W/m^2 due to shortwave and +0.18 W/m^2 due to longwave forcing. We decompose the shortwave forcing into component parts and find the direct radiative effect is the dominant component (+0.79 W/m^2), with a smaller contribution from semidirect effects (+0.54 W/m^2) partly countered by negative indirect effects (−0.29 W/m^2). The effective radiative forcing varies from 0.20 to 1.97 W/m^2 across a reasonable range of black carbon to total carbon emission ratios for the residential sector. Overall, this study shows that mitigation of the residential sector is likely a viable method to locally reduce short-term atmospheric warming in China, but efforts are needed to reduce uncertainty in composition of residential sector emissions to be confident in this conclusion.

1. Introduction

Atmospheric aerosols affect regional weather and climate through interactions with radiation and clouds, with the net impacts being sensitive to the chemical composition, size, and spatial distribution of the aerosol population (Boucher et al., 2013; J. Haywood & Boucher, 2000; Lee et al., 2016). Aerosols can both scatter and absorb solar radiation, resulting in the direct radiative effect (DRE). Black carbon (BC) is the aerosol component that absorbs the most radiation (Bond et al., 2013). Reducing BC emissions has therefore been proposed as a method to more rapidly reduce the impact of anthropogenic climate change compared to mitigation of long-lived greenhouse gasses (Anenberg et al., 2012; Jackson, 2009; Ramanathan & Carmichael, 2008; Shindell et al., 2012). However, BC is usually coemitted with other primary aerosol species, such as organic carbon (OC), and precursors to secondary aerosol species that predominantly scatter radiation (Bond et al., 2013). Aerosols also interact with clouds: By acting as cloud condensation nuclei (CCNs), aerosols adjust cloud optical properties and lifetime, causing the aerosol indirect effects (AIEs; Lohmann & Feichter, 2005; Myhre et al., 2013). The absorption of radiation also affects cloud formation causing adjustments to the aerosol-radiation interaction radiative forcing, also known as the semidirect radiative effect (SDRE; Allen & Sherwood, 2010; Koch & Del Genio, 2010; Ramanathan et al., 2001). Overall, aerosols are thought to have a net negative radiative forcing (cooling) effect on the world's climate, but with a high degree of spatial heterogeneity and the greatest contribution to uncertainty in estimates of anthropogenic radiative forcing (Myhre et al., 2013).

Emissions from the residential sector contribute substantially to the atmospheric aerosol burden, particularly where solid fuels are used for cooking and heating. In China, the residential sector contributes approximately 51% and 81% of total anthropogenic BC and OC emissions, respectively (Li et al., 2017). Aerosol emissions from inefficient cookstoves are important contributors to indoor and ambient air pollution, increasing premature mortality in adults and children (Archer-Nicholls, Carter, et al., 2016; Chafe et al., 2014; Cohen et al., 2017; Lelieveld et al., 2015; Liu et al., 2016; Naeher et al., 2007). The high BC content of residential emissions means that mitigation of this sector may also reduce short-term anthropogenic warming (Anenberg et al., 2012; Unger et al., 2010). However, aerosol emissions from the residential sector are subject to large uncertainties in their magnitude and composition (Akagi et al., 2011; Carter et al., 2016; Coffey et al., 2017; Secrest et al., 2017; Stockwell et al., 2015; Zhang et al., 2009). This combination of high uncertainty and high impact is driving research into improving estimates of residential sector emissions (Klimont et al., 2017; Zhang et al., 2018) and better understanding of their impacts on climate (Butt et al., 2016; Gao et al., 2018; Lacey & Henze, 2015; Li et al., 2015).

The impact of aerosols on climate is generally calculated using numerical model simulations of the atmosphere (e.g., Butt et al., 2016; Lacey & Henze, 2015; Unger et al., 2010). It is essential to perform global simulations over many decades to understand the long-term impact of aerosols on the Earth's climate, which limits such simulations to coarse (>100 km) spatial resolution. In recent years regional models, such as the Weather Research and Forecasting model with Chemistry (WRF-Chem; Grell et al., 2005) have enabled the detailed investigation of aerosol-radiation and aerosol-cloud interactions over specific parts of the world at higher (≤60 km) horizontal resolutions (Archer-Nicholls, Lowe, et al., 2016; Chapman et al., 2009; Fast et al., 2006; Grell et al., 2011; Saide et al., 2012; Yang et al., 2011), including over East Asia where large emissions of air pollutants cause high aerosol loadings and strong local radiative forcings (Chen et al., 2014; Gao et al., 2016, 2018; Huang et al., 2015; Yao et al., 2017).

In this study, we use the WRF-Chem model to investigate the radiative impact of residential sector aerosol emissions over China. The model is run for a monthlong case study in January 2014, when emissions due to the residential sector were high due to the contribution of heating emissions (for details on how the contribution of the residential sector to aerosol pollution in China changes through the year, please see Archer-Nicholls, Carter, et al., 2016). Model output is evaluated against surface observations and remote sensing products. We calculate the top-of-the-atmosphere (TOA) effective radiative forcing (ERF) of residential sector emissions over East Asia and break it down into component parts due to the DRE, AIE, and SDRE. We further test the sensitivity of our results to the uncertainty in emitted BC fraction by building on Lacey and Henze (2015), who derived a range of BC to total carbon emission ratios (BC:TC) from a literature review of measurements of BC and OC emission factors from cookstoves and used radiative forcing scaling factors to estimate the impact of this uncertainty on the global surface temperature. We apply the same emission fractionation as Lacey and Henze (2015) but use an online coupled model at higher resolution instead of a global off-line model to give a more detailed evaluation of the sensitivity of the regional climate in China to aerosol composition. We find a high sensitivity between uncertainty in BC content of residential sector emissions and their radiative forcing, with implications for potential mitigation strategies.

2. Materials and Methods

2.1. Model Description

The WRF-Chem model simulations in this study use the same domain and physical parameterizations as described by Archer-Nicholls, Carter, et al. (2016). However, to better represent aerosol interactions with radiation and clouds, we use the expanded Model for Ozone and Related Tracers gas-phase chemical mechanism (Emmons et al., 2010) with the four-bin Model for Simulating Aerosol Interactions and Chemistry (MOSAIC) aerosol scheme with aqueous chemistry (Zaveri et al., 2008), which includes some secondary organic aerosol (SOA) formation (Knote et al., 2014, 2015). MOSAIC uses a sectional representation of aerosol sizes, which enables the simulation of size distribution and number density of aerosols, critical parameters for calculating aerosol optical properties (Barnard et al., 2010) and their capacity to act as CCN and activate in clouds (Abdul-razzak & Ghan, 2002). The model is run with feedbacks between the chemistry and meteorology, allowing the aerosol fields to influence meteorological conditions through interactions with radiation and clouds, and vice versa (Chapman et al., 2009). One

limitation of the current WRF-Chem model is that aerosol particles cannot act as CCN in clouds simulated by the convective parameterization (the Grell 3-D scheme; Grell & Freitas, 2014; Grell & Devenyi, 2002). To explicitly resolve all clouds, the model must be run at high resolution (typically ≤4 km; Archer-Nicholls, Lowe, et al., 2016; Grell et al., 2011; Saide et al., 2012), which limits studies to short simulations (days). In this study, we choose to use a 27-km domain to make running simulations for a full month feasible.

China suffers from its worst air pollution events in wintertime due to the combination of meteorological conditions (Zhang et al., 2015; Zheng et al., 2015) and high residential sector emissions from heating (Carter et al., 2016; Streets et al., 2003). The month of January is therefore chosen as the study period when the greatest contribution of residential sector emissions to aerosol burden nationally is likely to occur, to maximize the strength of the signal. Model runs are conducted from 26 December 2013 to 1 February 2014, with output over January used for analysis. The year 2014 was chosen to be run in order to have good coverage from the China National Environmental Monitoring Center (CNEMC, http://www.cnemc.cn/) data set to evaluate surface $PM_{2.5}$ against, as described in Archer-Nicholls, Lowe, et al. (2016). The model domain is made up of 51 vertical levels and 200 × 155 cells at 27-km horizontal grid spacing over East Asia.

Meteorological initial and boundary conditions are derived from the European Center for Medium Weather Forecasts operational model analyses and products at 6-hourly intervals with horizontal grid spacing of 0.141° (http://www.ecmwf.int/), while chemical and aerosol boundary conditions are derived from the Model for Ozone and Related Tracers global chemical transport model (Emmons et al., 2010). The meteorological fields are reinitialized every 24 hr at 00:00 UTC (08:00 LT) to constrain dynamical divergence between scenarios, using the chemical and aerosol fields from the previous time step. The model is run for 36 hr after each reinitialization, giving a 12-hr overlap period where the previous leg is used for analysis while the next leg spins up.

2.2. Emission Scenarios

We use version 2.2 of the Emission Database for Global Atmospheric Research created as a part of the Hemispheric Transport of Air Pollutants providing monthly anthropogenic emissions representative of the year 2010, the most recent available when the simulations were conducted (Janssens-Maenhout et al., 2012, 2015). The Emission Database for Global Atmospheric Research created as a part of the Hemispheric Transport of Air Pollutants inventory is itself a gridded MOSAIC of regional inventories, using the Multi-Resolution Emission Inventory for China (MEIC; http://www.meicmodel.org/), part of the MIX inventory for Asia (Li et al., 2017). The MEIC emissions for each sector are calculated bottom-up using activity factors and emission factors for different technologies derived from a wide range of data sources (Li et al., 2017; Zhang et al., 2007, 2009).

In China, the majority of residential aerosol emissions are due to inefficient combustion of solid coal and biofuels for cooking and heating purposes, contributing some 51% and 81% of total BC and OC emissions, respectively (Li et al., 2017). Other contributions to the residential sector includes emissions from other fuel sources, such as liquified petroleum gas, and other activities, such as lighting (Klimont et al., 2017). The type of fuel burned and corresponding emission factors vary across China: In the South and West biofuels such as wood and agricultural waste are used, while in the North coal usage is more common. The temporal activity of these emissions is determined based on a parameterizations (Bond et al., 2007; Streets et al., 2003) that modify the residential sector emissions based on monthly average temperature by province such that emissions peak over winter due to the additional contribution of heating (Archer-Nicholls, Carter, et al., 2016). Note that because emissions are calculated for the whole year then modulated by sector to give monthly varying emissions, relative ratios of different emission components from the residential sector do not change over the year. Each sector also follows a different diurnal profile for emission flux (Olivier et al., 2003), and vertical mixing is applied to the power sector following Wang et al. (2010).

We also include emissions from nonanthropogenic sources. Emissions of biogenic compounds are calculated online using the Model of Emissions of Gases and Aerosols from Nature (version 2; Guenther et al., 2012). Open fire emissions from wildfires, agricultural, and prescribed burnings are taken from the Fire Inventory from National Center for Atmospheric Research (version 1.5; Wiedinmyer et al., 2011). Biogenic and biomass burning emission sources are less significant over the winter time period studied:

Table 1
Table of Model Simulation Scenarios Conducted for Study

Scenario	Residential emissions	BC:TC[a] ratio (Φ)
BASE	True	Standard (0.24)
NORES	False	N/A
LOWBC	True	Low (0.15)
HIGHBC	True	High (0.33)

Note. HIGHBC = high BC:TC ratio.

Agricultural fires in East Asia are most prevalent in late spring and autumn (J. Li et al., 2016) and biogenic emissions are strongest in summer (Guenther et al., 2012).

Four emission scenarios are simulated as summarized in Table 1. The BASE scenario uses all anthropogenic emissions, while NORES excludes emissions from the residential sector. To test sensitivity to the uncertainty in the fraction of BC emissions, the average black carbon to total carbon (BC:TC) ratio of residential sector emissions is changed to a "high BC:TC ratio" (HIGHBC) of 0.33 and a "low BC:TC ratio" (LOWBC) of 0.15, respectively, compared to an average in the BASE scenario of 0.24. The range in BC:TC ratios is one standard deviation above and below the mean of multiple measurements of OC and BC emissions from field and laboratory measurements of cookstoves from across the world, including four targeting specific fuels used in China, as compiled by Lacey and Henze (2015). While new measurements of BC and OC emission factors from cookstoves and other residential sources have been conducted since the publication of Lacey and Henze (2015), incorporating these new data does not have a significant impact on the mean and standard deviation of the collective data (see Figure S1 in the supporting information). What limited measurements of residential emissions that have been conducted show a wide range of BC:TC emission ratios (Bond et al., 2013; Coffey et al., 2017; Lacey & Henze, 2015); the range used for this study covers a valid representation given current understanding. The average BC:TC of emissions from the MEIC inventory, used as part of EDGAR_HTAP inventory in the study, is 0.24, the same as the average from Lacey and Henze (2015) despite being independently developed. The review by Bond et al. (2013) shows that BC:TC ratios from energy sources (including both biofuel and fossil fuel use) from different emission inventories range from 0.22 to 0.36 over China. A recent study by Zhang et al. (2018) found emissions of BC from rural biomass and coal use in China to be 640 ± 245 Gt/year, a range of uncertainty that is equivalent to that tested in this study. We therefore use the same range as in Lacey and Henze (2015) to enable comparability with their study.

The residential sector emissions of BC and OC are scaled at each grid point via

$$E^{*}_{RES,BC} = E_{RES,BC} \times \left(\frac{\Phi}{0.24}\right), \quad (1)$$

$$E^{*}_{RES,OC} = E_{RES,OC} \times \left(\frac{1-\Phi}{1-0.24}\right), \quad (2)$$

where Φ is the new BC:TC emission ratio (0.33 and 0.15 for HIGHBC and LOWBC scenarios, respectively).

While we acknowledge that there is uncertainty in the total amount of carbon emissions from the residential sector, these experiments have been designed to test sensitivity to the aerosol BC fraction only. As the average BC:TC ratio over China in the EDGAR_HTAP base inventory is 0.24, the same as the average in Lacey and Henze (2015), the HIGHBC and LOWBC scenarios have the same total emitted primary aerosol mass as the BASE scenario over China. However, due to variations in emission factors, there are small, unavoidable differences in emitted aerosol mass in some regions (see Figures S2 and S3). Another consequence of this approach is that we cannot scale OC emissions by some factor (typically between 1.4 and 2.1; Turpin & Lim, 2001) to give total organic aerosol mass accounting for associated hydrogen and oxygen. The scaling of OC emissions would result in greater total primary aerosol emissions in the LOWBC scenario and negative emissions of "other inorganics" (calculated as the remaining primary $PM_{2.5}$ emissions after removing BC and organic aerosol emissions), which in turn would prevent us from testing the sensitivity to the emitted BC fraction only. However, the lack of OC emission scaling should have little impact on the conclusions drawn from this study, as the physical properties of OC and other inorganic aerosols are similar within the MOSAIC aerosol mechanism. This omission has no impact on the amount of SOA generated.

2.3. Calculation of Radiative Effects

Calculating the radiative effects of aerosols follows the same methodology as described in Archer-Nicholls, Lowe, et al. (2016). Briefly, Mie calculations are first used to calculate aerosol optical properties. The complex refractive index of each aerosol bin is approximated using the Maxwell-Garnett method whereby aerosols are assumed to contain randomly distributed BC spheres among a mixture of all other components

(Bohren & Huffman, 1983, chapter 8). This approximation avoids the known biases of volume-averaging and external mixing rules (Bond et al., 2006).

Radiative transfer is calculated at four shortwave wavelengths (300, 400, 600, and 1,000 nm) and 16 longwave wavelengths using the Rapid Radiative Transfer Model for Global applications parameterization (Iacono et al., 2000). We use double-radiation calls to calculate "clean-sky" diagnostic radiation fluxes, which ignore aerosol-radiation interactions but include the effects of clouds, in addition to full radiation fluxes, which include the effects of both aerosols and clouds. The radiative forcing due to residential aerosol emissions is calculated as the difference in shortwave and longwave radiation flux at the TOA between the BASE and NORES scenarios ($\Delta SW^{\uparrow}_{TOA}$ and $\Delta LW^{\uparrow}_{TOA}$, respectively). A positive value means that the residential emission source results in more radiation being absorbed than would occur if there were no residential emissions, resulting in warming of the atmosphere. Following the methods of Ghan et al. (2012), as implemented in WRF-Chem by Archer-Nicholls, Lowe, et al. (2016), we use the clean-sky and full radiative fluxes to decompose $\Delta SW^{\uparrow}_{TOA}$ into three components: (1) those due to aerosol-radiation interactions (or DRE), (2) those due to rapid responses to aerosol direct radiative forcing (the SDRE), and (3) those due to aerosol modification of cloud optical properties and lifetime (the AIE).

Since the model simulations have their meteorological fields reinitialized every 24 hr and the boundary conditions are driven an independent global model, the local aerosol radiative forcings do not affect large-scale dynamics or ocean temperatures and should therefore not be confused with the long-term "stratospherically adjusted radiative forcing" as defined by the Intergovernmental Panel on Climate Change (Myhre et al., 2013). However, the aerosol fields do cause rapid readjustments in atmospheric temperature, water vapor, and cloud fields. The net aerosol radiative forcing ($\Delta SW^{\uparrow}_{TOA}$) is therefore closest to the Intergovernmental Panel on Climate Change definition of ERF. The necessarily limited time scale and area of our regional model runs do mean the results presented are not exactly equivalent to ERF as calculated by global climate models but are informative in demonstrating the short-term local impacts of aerosols on weather and climate.

2.4. Description of Observational Datasets

The CNEMC (http://www.cnemc.cn/) provides an extensive network of air quality monitoring stations consisting of approximately 900 sites in 187 cities across China during the period of study. Each station measures $PM_{2.5}$, PM_{10}, NO_2, CO, O_3, and SO_2. For this study, daily average surface $PM_{2.5}$ concentrations are used for model evaluation. For instances where multiple sites fall within the same WRF-Chem grid cell, observational data are averaged prior to comparison. Data were downloaded from http://pm25.in/, a direct mirror site of CNEMC. For more detail and previous analysis of the data set, please see, for example, Rohde and Muller (2015).

To evaluate the optical properties of aerosol in the WRF-Chem simulations, we compare model output with various remote sensing products. Model output with data from the Moderate Resolution Imaging Spectroradiometer (MODIS; Remer et al., 2005) instrument on board the Terra satellite. The product used was the Aerosol Optical Thickness at 550 nm for both ocean (best) and land (corrected) at 1° resolution (MOD08_M3_v6) mean for the month of January 2014. The data set was downloaded from the Level-1 and Atmosphere Archive & Distribution System Distributed Active Archive Center, located in the Goddard Space Flight Center in Greenbelt, Maryland: ladsweb.modaps.eosdis.nasa.gov/ (last accessed 3 December 2018). For comparison, we used the WRF-Chem diagnostic extinction at 550-nm variable summed through the atmospheric column to give aerosol optical depth (AOD) at 550 nm.

To further evaluate the absorption of the aerosol model fields, we compare against several Aerosol Robotic Network (AERONET) sites across China (N. Holben et al., 2001). For comparison, we used the Version 3 Direct Sun and Inversion Algorithm for AOD, single scattering albedo (SSA) and absorbing aerosol optical depth (AAOD), all at 440 nm (Andrews et al., 2017). To compare against the model, AOD and SSA were calculated at 440 nm using the WRF-Chem diagnostic variables at 400 and 600 nm using the Ångström exponent also calculated between the range 400–600 nm. SSA was calculated as an extinction-weighted column average. The AAOD, defined as the fraction of AOD that absorbs radiation, was calculated as

$$AAOD = AOD \times (1 - SSA) \quad (3)$$

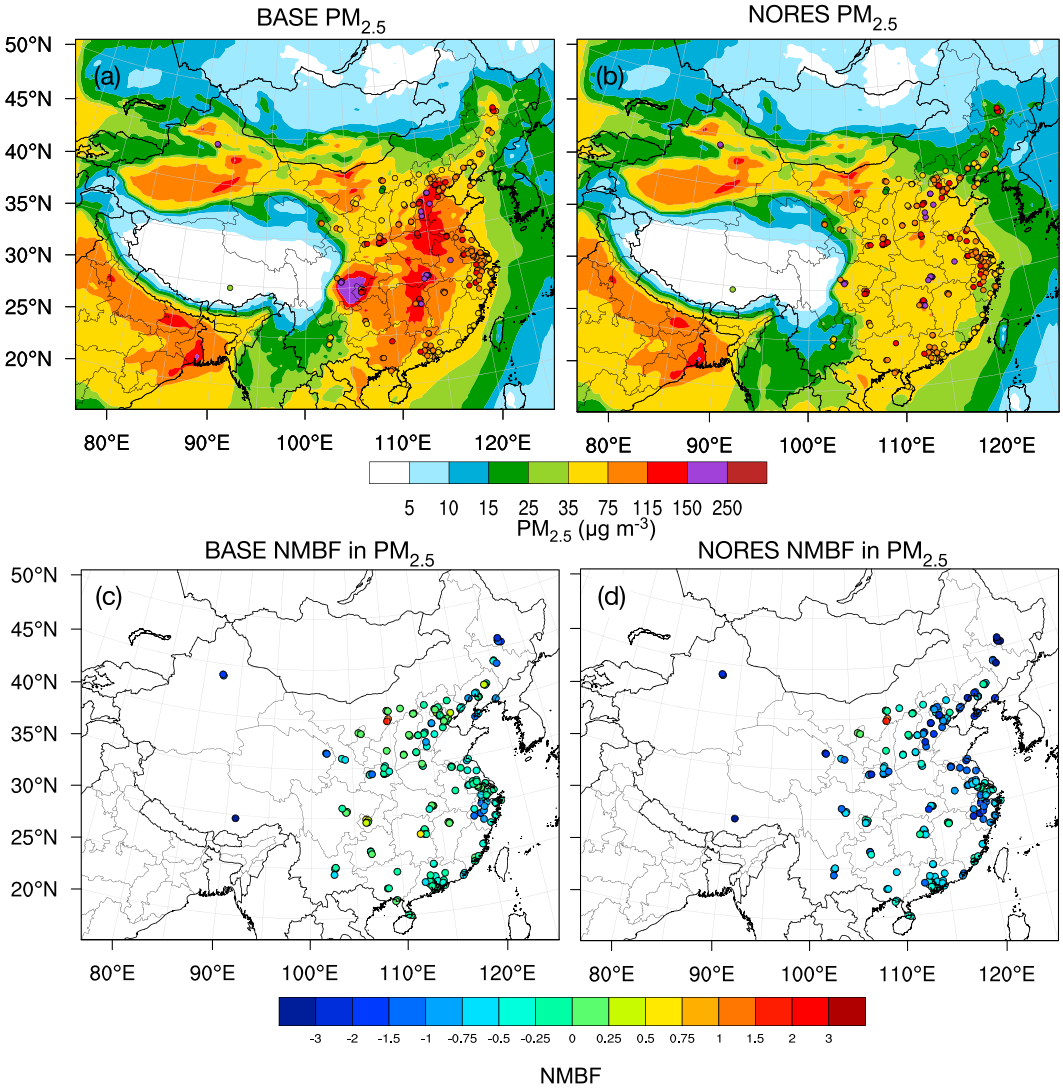

Figure 1. Comparison of average surface $PM_{2.5}$ from BASE (a) and NORES (b) model scenarios with observations from the CNMEC database over January 2014. (c) and (d) show normalized mean bias factor (NMBF) between the BASE and NORES runs, respectively, with observations at each measurement site. Red colors indicate locations where the model is biased high, blue where the model is biased low, and green where model and observations are similar.

Due to lack of level 2 data over the period studied, we had to use level 1.5 data, which have been screened for clouds but have greater associated uncertainties that should be acknowledged (Andrews et al., 2017). Data were downloaded from https://aeronet.gsfc.nasa.gov/cgi-bin/webtool_inv_v3 (last accessed 3 August 2018). Due to limited data over the time period studies (January 2014), only four sites were deemed to have sufficient data to be worth analyzing. The locations of the four sites are plotted in Figure S4.

3. Model Evaluation

3.1. Surface $PM_{2.5}$

Monthly average $PM_{2.5}$ from BASE and NORES model scenarios is compared with the CNEMC database in Figure 1. $PM_{2.5}$ concentrations in the HIGHBC and LOWBC scenario are similar to the BASE scenario (Figure S2). Bias between the model and observations is calculated using the normalized mean bias factor (NMBF), as defined by (Yu et al., 2006):

$$\mathrm{NMBF} = \frac{\overline{M}}{\overline{O}} - 1, \quad \text{if } \overline{M} \geq \overline{O}, \text{and } \mathrm{NMBF} = 1 - \frac{\overline{O}}{\overline{M}}, \quad \text{if } \overline{M} < \overline{O},$$

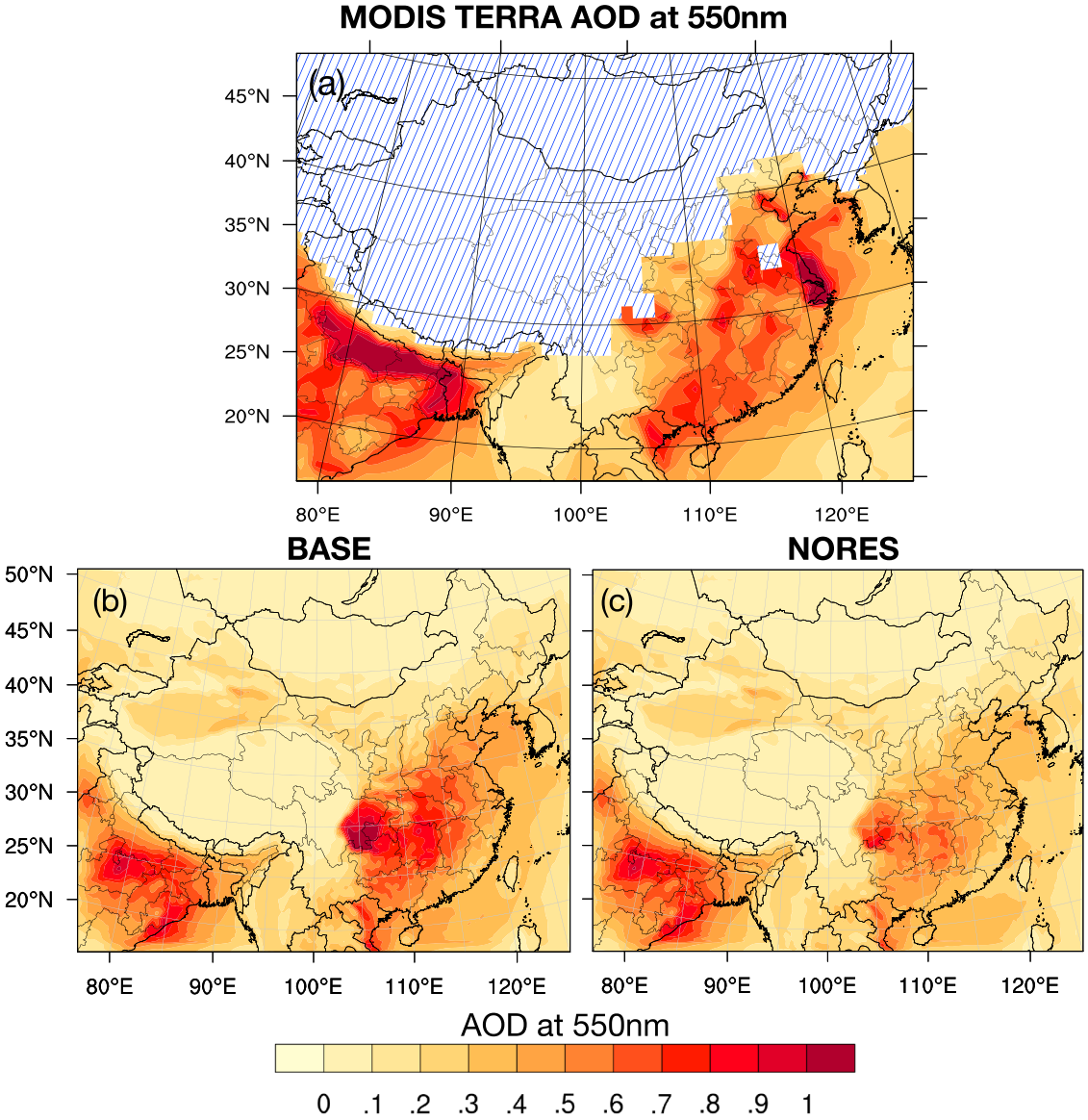

Figure 2. Aerosol optical depth aerosol optical depth (AOD) (a) at 550 nm averaged over month of January from Moderate Resolution Imaging Spectroradiometer (MODIS) Terra satellite MOD08_M3 product. January 2014 average AOD for BASE (b) and NORES (c) scenarios.

where M^- and O^- are the mean modeled and observed values, respectively. In the BASE scenario (Figure 1c), the model is biased low in the remote regions of West and North-West China, which are dominated by dust aerosols (S. Chen et al., 2014). It is also biased low compared to many of the sites in Eastern China, where there are many large cities with high anthropogenic emissions. Over much of the rest of China, the BASE simulation compares well with surface observations of $PM_{2.5}$. The NORES scenario is biased low for surface $PM_{2.5}$ over much of the country (Figure 1d), emphasizing the importance of including residential sector emissions to accurately simulate the aerosol burden over China.

3.2. Aerosol Optical Properties

Modeled AOD is compared against the MODIS AOD product from the Terra satellite (Remer et al., 2005) for the month of January 2014 in Figure 2. Details of the data used for evaluation are given in the section S3. AOD for the HIGHBC and LOWBC scenarios are almost identical to the BASE scenario, showing little sensitivity to the composition of the aerosol (Figure S5). While the overall magnitude of AOD in the BASE model output is comparable to that observed by MODIS, there is a low model bias over Northern China

and the Eastern seaboard, and a high bias around Sichuan and central China. Interestingly, the BASE scenario has similar surface $PM_{2.5}$ to observations over the Western Sichuan province (Figure 1), where it also overestimates AOD compared to the MODIS data (Figure 2). This discrepancy highlights that surface $PM_{2.5}$ is not the only factor driving AOD. Either the model has too much aerosol in the vertical column above this region or errors in calculations of aerosol optical properties are causing a high AOD bias. The low bias in AOD Northern and Eastern China also correlates with a low bias in $PM_{2.5}$ and may be due to underestimation of emissions, the misrepresentation of distribution or speciation of emissions, underestimation of secondary aerosol formation, not enough water associated with aerosols, poor aerosol optical property calculations, or a combination of these factors.

To further evaluate the optical properties of aerosols in the modeling domain, in Figure 3 we compare model output with data from the AERONET (Andrews et al., 2017; Holben et al., 1998) at several sites for which data were available over the time period (see section S3 and Figure S4). Statistics calculated include mean bias (MB), mean absolute gross error, and correlation coefficient (R) as defined in Yu et al. (2006). Due to limited available data, these results are only valid over the sites analyzed and may not be representative of the rest of China. The model simulations generally compare well to AERONET observations, but there are some systematic biases. AOD is lower in the BASE scenario compared to observations. AOD in the HIGHBC and LOWBC scenarios is very similar to BASE, but significantly lower in NORES. The BASE model runs are also low in SSA compared to observations, meaning that the modeled aerosol is more radiatively absorbing than that observed. SSA is lower still in the HIGHBC scenario and closer to observations in the LOWBC and NORES scenarios, showing that the variation in BC content of residential sector emissions has a large impact on how radiatively absorbing the aerosol population is. However, even in the LOWBC and NORES scenarios, where there is significantly less BC aerosol, the model runs are still biased slightly low in SSA (Figures 3h and 3k). The BASE scenario does compare well for AAOD (Figure 2c); in fact, the MB is negligible. However, it is likely the model is generating a good result for the wrong reasons: the low biases for AOD and SSA roughly cancel each other out given how AAOD is defined in equation (3). Nonetheless, the comparison suggests that the model is representing the net radiative impact of the aerosol layer well.

The biases in AOD and SSA can be explained if there are missing processes in the model or errors in calculation of aerosol optical properties. Realistically resolving the mixing state of BC with other aerosol species is a key computational challenge (Kodros et al., 2018; Matsui et al., 2013). We use a Maxwell-Garnett approximation, which avoids the known biases of a volume-mixing or external-mixing rules (Barnard et al., 2010). Explicit simulation of BC mixing state in aerosol particles has recently been shown to have a large impact on the sensitivity to BC radiative forcing (Matsui et al., 2018); however, inclusion of this capability is beyond the scope of this study. WRF-Chem also assumes organic aerosol is nonabsorbing, even though recent evidence suggests some (known as brown carbon [BrC]) partially absorbs SW radiation (Andreae & Gelencs, 2006; Lack et al., 2012; Yao et al., 2017). BrC has been identified from residential sources, but there is large uncertainty related to the optical properties and atmospheric aging of BrC (Chen et al., 2017; Stockwell et al., 2015; Sun et al., 2017). However, the inclusion of BrC would lower SSA, increasing the magnitude of the current biases. Finally, the model likely underestimates the contribution of SOA, and there is mounting evidence that some heterogeneous chemical processes, not currently represented in WRF-Chem, enhance secondary aerosol formation and are critical for forming the winter haze events observed in North and East China (Chen et al., 2016; Gao et al., 2017; Li et al., 2018; Zhang et al., 2015). Overall, these added processes would likely increase simulated AOD and SSA, which would reduce the biases of the BASE scenario compared with AERONET observations (Figure 3), but would not necessarily change the conclusions of this study since residential emissions would similarly add BC to the aerosol population, increasing the absorption of aerosols relative to the NORES scenario.

4. Results

Aerosols can influence local weather systems and climate through their interactions with radiation and clouds. Whether an aerosol layer has a positive of negative DRE, as seen from the TOA, depends on both the SSA of the aerosols and the albedo of the surface the aerosol layer is over (Haywood & Shine, 1995). However, in either case an absorbing aerosol layer will always reduce incident radiation at the surface,

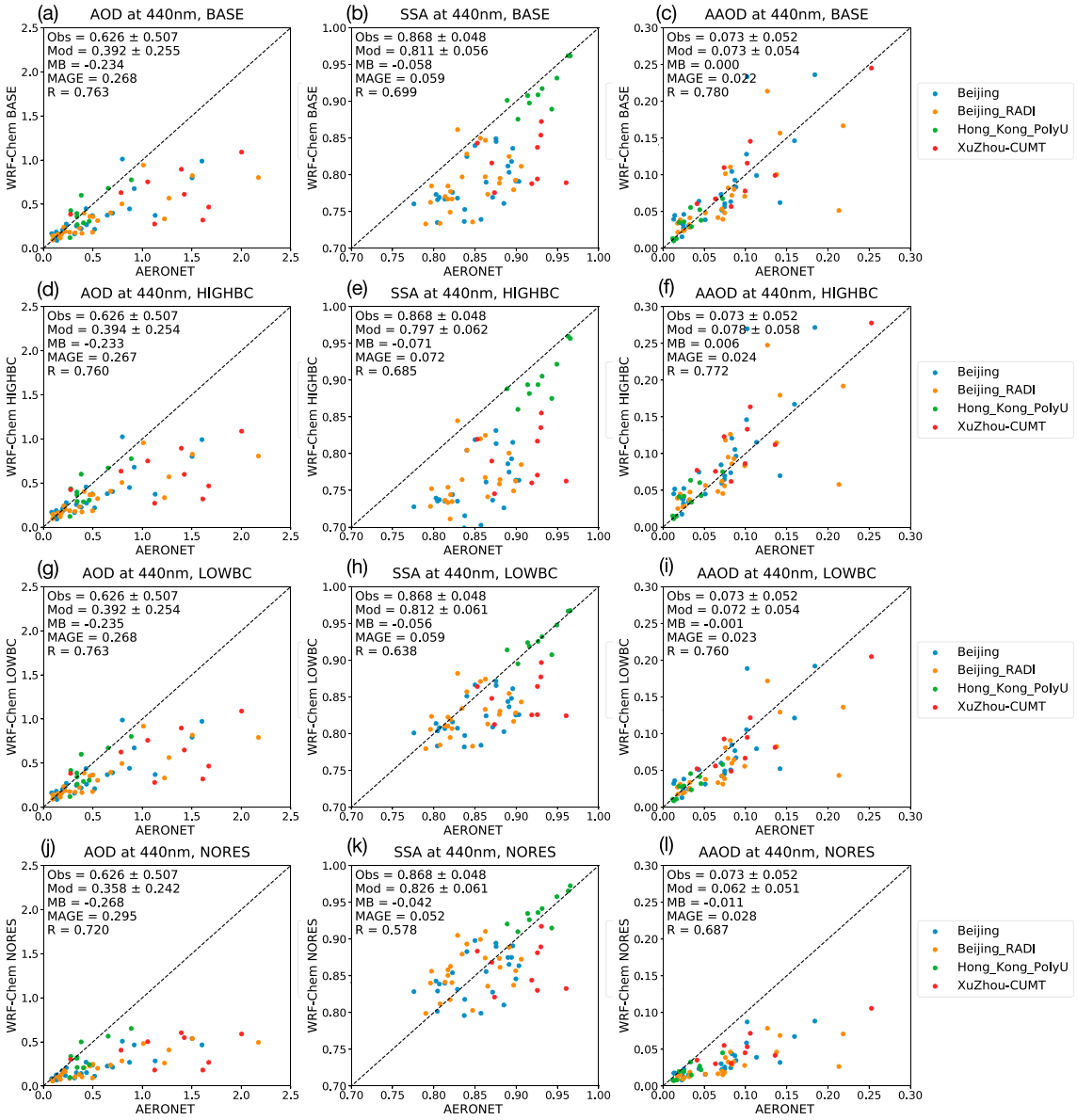

Figure 3. Scatterplots comparing daily average derived aerosol optical data from Aerosol Robotic Network (AERONET) sites in China with Weather Research and Forecasting model with Chemistry (WRF-Chem) model data over the month of January 2014. Dashed black line shows 1:1 line between model and observations. Comparing aerosol optical depth (AOD) at 440 nm (left column), single scattering albedo (SSA) at 440 nm (middle column), and absorbing aerosol optical depth (AAOD) at 440 nm (right column) for each of the four scenarios: (a–c) BASE, (d–f) high BC:TC ratio (HIGHBC), (g–i) low BC:TC ratio (LOWBC), (j–l) and NORES. Legend for each panel shows means and standard deviation for observations and model, mean bias (MB), mean absolute gross error (MAGE), and Pearson's correlation coefficient (R; Yu et al., 2006).

cooling the lowest levels of the atmosphere, and absorb more radiation through the atmospheric column (Figure 4). In each of the scenarios with residential emissions (BASE, HIGHBC, and LOWBC), there is a decrease in downwelling surface radiation and an increase in radiation absorbed by the atmospheric column compared to the scenario with no residential emissions (NORES). The surface reduction in SW radiation is greatest in the HIGHBC scenario, but this scenario also absorbs the most radiation in the atmospheric column. The mitigation of residential emissions may therefore be perceived as an increase in surface temperature, even if the net energy absorbed by the atmosphere is decreased.

The ERF of residential sector emissions is calculated as the difference in TOA radiative flux between the scenarios with residential emissions (BASE, HIGHBC, and LOWBC) and the run without (NORES). Results are summarized in Table 2, showing average ERFs of the residential sector over the whole

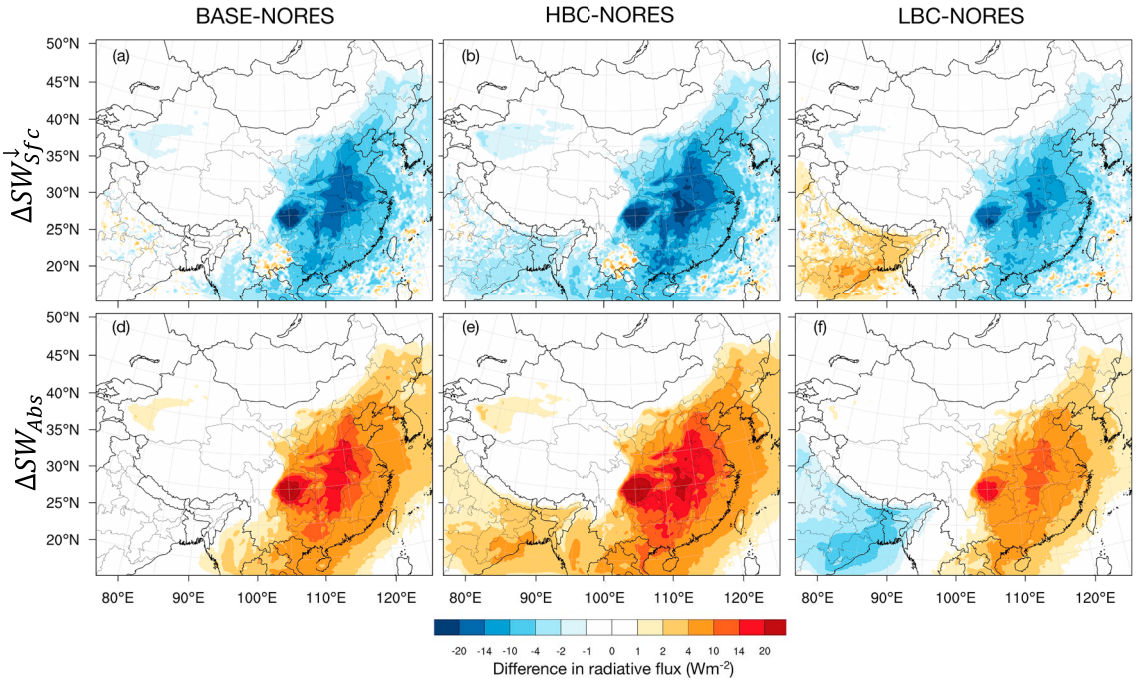

Figure 4. Difference in downwelling SW radiation at surface between BASE and NORES (a), high BC:TC ratio (HBC) and NORES (b), and low BC:TC ratio (LBC) and NORES scenarios (c). Difference in SW radiation absorbed by atmospheric column between BASE and NORES (d), HBC and NORES (e), and LBC and NORES scenarios (f). Figures show average values for the month of January 2014.

domain (ignoring the outmost five grid cells in each direction to avoid boundary effects) and over the "East China" region of the of the domain (20°N 100°E and 45°N 120°E). As the East China region covers the whole land area where most residential emissions in China occur, avoiding the North Eastern part of India, and encompasses the majority of the Chinese population, the rest of the analysis will focus on this subregion (shown in Figure S4).

Table 2
Average ERFs (in W/m^2) at TOA Relative to NORES Scenario Averaged Over Whole Domain (Excluding the five Outermost Grid Cells in Each Dimension) and Over East China Region of Domain (20°N 100°E to 45°N 120°E, shown in Figure S4)

	BASE		HIGHBC		LOWBC	
Region	Whole domain	East China	Whole domain	East China	Whole domain	East China
Net total	+0.49	+1.22	+0.94	+1.97	−0.09	+0.20
$\Delta SW_{TOA}^{\uparrow}$	+0.45	+1.04	+0.89	+1.77	−0.13	+0.05
$\Delta LW_{TOA}^{\uparrow}$	+0.04	+0.18	+0.05	+0.20	+0.04	+0.15
DRE	+0.32	+0.79	−0.68	+1.38	−0.16	−0.01
AIE	−0.12	−0.29	−0.11	−0.27	−0.13	−0.29
SDRE	+0.25	+0.54	+0.32	+0.66	+0.35	+0.35

Note. ERF = effective radiative forcing; TOA = top of the atmosphere; HIGHBC = high BC:TC ratio; LOWBC = low BC:TC ratio; DRE = direct radiative effect; AIE = aerosol indirect effect; SDRE = semidirect radiative effect. Net total is defined as the sum of $\Delta SW_{TOA}^{\uparrow}$ and $\Delta LW_{TOA}^{\uparrow}$. DRE, SDRE, and AIE are decompositions of the $\Delta SW_{TOA}^{\uparrow}$ forcing only.

The shortwave ($\Delta SW_{TOA}^{\uparrow}$) effects of aerosol attributable to the residential sector dominate over the longwave ($\Delta LW_{TOA}^{\uparrow}$) effects. The average $\Delta SW_{TOA}^{\uparrow}$ from the BASE scenario is +1.04 W/m^2 over East China, showing that residential sector aerosol emissions have a local net warming impact on the atmosphere. The absorbing BC components of residential sector emissions overwhelms the scattering effects of coemitted primary species such as OC and secondary aerosol forming species such as SO_2 and NOx (although the residential sector is a small source of NOx and SO_2 relative to industry, power, and transport; Li et al., 2017). The magnitude of $\Delta SW_{TOA}^{\uparrow}$ is greatest over the Sichuan Basin region of China, although the model does show a high AOD bias in this region (Figure 2). This radiative impact is highly sensitive to the BC content of residential sector aerosol emissions. The HIGHBC scenario (Figure 5b) exhibits a stronger warming over the East China region (+1.77 W/m^2), whereas in the LOWBC scenario (Figure 5c), the effect is largely neutral (+0.048 W/m^2).

We further decompose $\Delta SW_{TOA}^{\uparrow}$ into DRE, SDRE, and AIE components in Figures 5d–5l. The majority of the warming in the BASE and HIGHBC scenarios is due to the DRE (0.79 and 1.37 W/m^{2}1, respectively), whereas there is no net warming in the LOWBC scenario (−0.01 W/m^2). The AIE is similar in all of the scenarios (−0.29 W/m^2), indicating that aerosol-cloud interactions are more sensitive to the total aerosol burden than to the BC

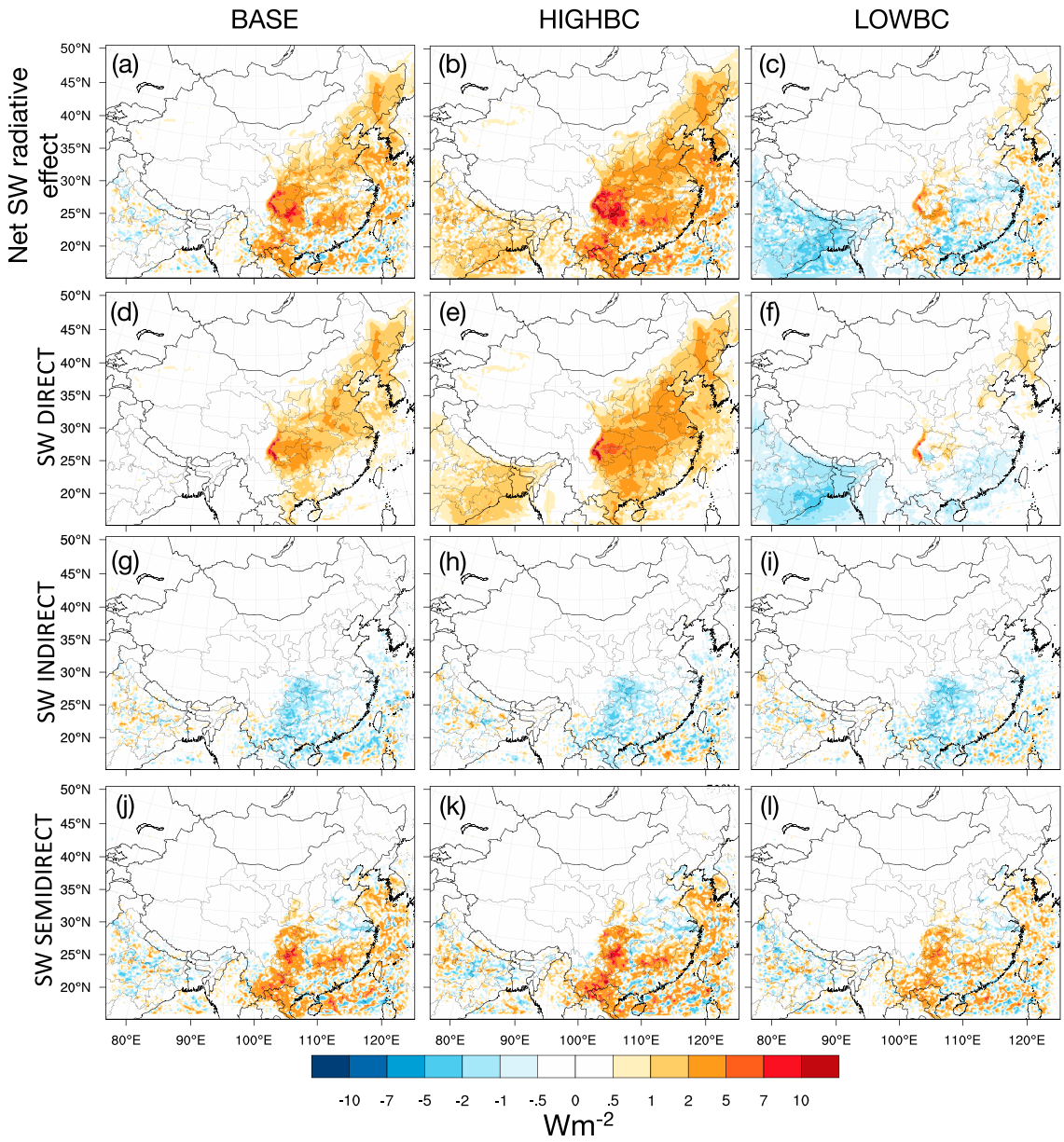

Figure 5. Top row: effective radiative effect of residential emissions calculated as difference in top-of-the-atmosphere SW radiation flux ($\Delta SW^{\uparrow}_{TOA}$) between BASE and NORES (a), high BC:TC ratio (HIGHBC) and NORES (b), and low BC:TC ratio (LOWBC) and NORES (c). Lower figures show decomposition of $\Delta SW^{\uparrow}_{TOA}$ into direct radiative effect (direct radiative effect; d–f), aerosol indirect effect (g–i), and semidirect radiative effect (j–l).

content of the aerosol (Figures 5g–5i). The SDRE shows a similar spatial distribution in all three cases, with most warming over Southwest China, again in regions with both high cloud cover and aerosol burden (Figures 5j–5l). The magnitude of the SDRE effect is greatest in the HIGHBC scenario (0.66 W/m^2) and weakest in the LOWBC scenario (0.35 W/m^2). The SDRE is highly varied across the domain compared to the DRE, negative in many regions, highlighting the complex nature of this effect. However, the similar spatial distribution in BASE, HIGHBC, and LOWBC of the AIE and SDRE shows a strong consistency in short-term cloud response to aerosol.

Several recent studies, mostly using global models, have focused specifically on the impact of BC and residential emissions on climate (e.g., Aunan et al., 2009; Butt et al., 2016; Kodros et al., 2015; Lacey & Henze, 2015). Using the GEOS-Chem model, Lacey and Henze (2015) estimated a total contribution to net global warming from cookstove emissions of 33 mK with model DRE and parameterized AIE. Using

the same range of BC:TC emission factors, they also found the range of impacts to span zero. Kodros et al. (2015) used a cloud-resolving version of GEOS-Chem and estimated the global impacts of annual biofuel emissions results in an ERF of +0.35 W/m^2. Butt et al. (2016) in contrast found the residential sector emissions to have a slightly negative DRE globally using the GLOMAP chemical transport model, with East Asia being a key region of negative forcing, as well as a strongly negative indirect effect. There are multiple reasons why they found a different result to other publications such as different emission inventory, errors in optical properties, and assumptions of aerosol size distribution and mixing state. Recently, Gao et al. (2018) assessed the DRE of multiple sectors over China and India using the WRF-Chem model. They found the residential sector to have a radiative forcing of 0.97 W/m^2 over China from both SW and LW, similar to the 1.22 W/m^2 from the BASE scenario over the East China region of the domain in this study. Like Gao et al. (2018), we find the LW forcing is positive but smaller in magnitude to the DRE. However, we also find the net total impact to be amplified when considering the SDRE and AIE as well, effects that were not considered by Gao et al. (2018).

5. Conclusions

Emissions from the residential sector are a major source of particulate matter in China, and their removal would therefore greatly lower the aerosol burden and AOD (Figure 1). The high BC content of residential emissions produces aerosol particles that absorb SW radiation, lowering the SSA and increasing the AAOD of the aerosol population. Evaluating the difference in radiative flux at the TOA between the BASE and NORES simulations shows residential sector emissions cause net instantaneous positive forcing, as more SW radiation is absorbed by the atmosphere (Figure 4). We further decompose the ERF of aerosols from residential emissions into DRE, SDRE, and AIE to gain a more detailed understanding aerosol-cloud-radiation interactions. Overall, the net ERF over East China is 1.22 W/m^2 with the SW DRE the largest component contributing 0.79 W/m^2 (Table 2). These values are large but comparable to similar studies in the region. However, the inclusion of cloud responses suggests further warming attributable to the SDRE that will not have been accounted for by previous studies focusing on the DRE.

Residential sector emissions are challenging to quantify reliably because of the wide range of imperfect conditions under which fuels are burned, limited emissions measurements (particularly field measurements of cookstoves being used under realistic conditions), and limited data on activity usage (Carter et al., 2016; Coffey et al., 2017; Secrest et al., 2017). We probe this uncertainty using sensitivity scenarios with low and high BC:TC ratio of residential sector emissions, using the range of estimates compiled by Lacey and Henze (2015). Within this reasonable range of BC:TC emission ratios, the net ERF of residential sector aerosol emissions in East China varies from near zero in the LOWBC scenario (0.20 W/m^2) to extremely high in the HIGHBC scenario (1.97 W/m^2). The majority of this sensitivity is due to changes in the DRE (increase of 75% from BASE to HIGHBC scenario) and partially due to changes in the SDRE (22% increase). In contrast, the AIE is largely insensitive to aerosol BC:TC ratio. These results suggest that mitigating residential sector emissions is a viable option to reduce atmospheric warming in East Asia, but due to the uncertainty in BC content of residential emissions, we cannot with confidence say this will definitely be the case. This finding highlights the impotence of understanding aerosol composition as well magnitude of emissions.

Our use of a regional model necessarily limits the study to be only valid for the time period and region studied. In choosing a winter case study, the contribution of residential sector emissions to the aerosol burden is at its greatest due to the contribution of heating emissions and less competition from other large aerosol sources (such as agricultural burning). The results presented therefore represent the likely maximum impact of residential emissions compared to other seasons. In other times of the year, one would expect the composition of aerosol emissions from the residential sector to change due to the different burn conditions of cooking and heating, but this is not currently represented in emission inventories. Understanding how the impact of the residential sector changes over the year can be the subject of future study. There may also be further long-term benefits from reduced coemitted greenhouse gas emissions (Bailis et al., 2015) and reduction in BC deposition on snow and ice (Lau et al., 2018), impacts which are beyond the scope of this study to investigate.

Emissions in China are changing rapidly, affecting the conclusions that can be drawn from studies such as this. While emissions for the year 2010 were the most up-to-date available when conducting the simulations

for this study, it should be noted that there have been rapid changes to emissions of aerosols and aerosol precursors in China, particularly post-2013 when new clear-air action policies were introduced. Zheng et al. (2018) document these changes to the MEIC inventory. Between 2010 and 2014 reductions have been most rapid for SO_2 emissions (−27%), largely driven by changes to the power sector, while reductions in OC and BC emissions from the residential sector have been more modest. Therefore, while accounting for changes in emissions between 2010 and 2014 would affect the modeled aerosol mass burden and composition, the contribution due to the residential sector would be broadly similar. However, Zheng et al. (2018) also showed that clean-air policy to switch residential coal use to gas and electricity, implemented after 2013, successfully reduced BC and OC emissions from the residential sector by approximately −25% and −30%, respectively, between 2013 and 2017.

Uncertainty in modeling of aerosol radiative forcing is high, particularly relating to the semidirect effects (also known as rapid adjustments). The semidirect forcing tends to only be positive over limited continental regions, with the global net effect often negative and therefore acting counter to the positive direct radiative forcing (Stjern et al., 2017; Y. Yang et al., 2019). The strength of the semidirect effect is also highly variable between models (Stjern et al., 2017) and nonlinearly dependent on the magnitude of BC emissions (Y. Yang et al., 2019). We therefore recommend similar studies to this paper are repeated on other regional models to be confident in the findings.

Mitigation of residential emissions is urgently needed to reduce aerosol loadings in many countries to counter the severe negative public health impacts of air pollution. Our results suggest that reducing residential solid fuel use is also a viable approach to reduce short-term local atmospheric warming; that is, there are potential climate cobenefits. The instantaneous TOA radiative forcing is largely driven by shortwave absorption by BC, causing a positive DRE. We also find a positive SDRE, as cloud cover is reduced due to increased BC, while the negative AIE is small over the time and region studied. The ERF is sensitive to the BC content of residential sector emissions, ranging from near zero to almost double the baseline over a reasonable range of BC:TC emission ratios. More work is therefore needed to improve carbonaceous emissions from the residential sector, including detailed lab and on-site measurements of cookstoves being used in real-world contexts. In addition, the potential benefits of mitigation of aerosol emissions from the residential sector are expected to be short term and local, so should not distract from mitigation of long-lived greenhouse gasses. However, as many households in Northern China burn coal for cooking and heating, and biofuel usage has also been shown to have a significant carbon footprint (Bailis et al., 2015), mitigation of BC emissions from the residential sector could be conducted in parallel with wider policy to reduce greenhouse gas emissions.

Acknowledgments
This study was supported by the U.S. Environmental Protection Agency Science to Achieve Results program Grant R835422. The Terra/MODIS Aerosol Cloud Water Vapor Ozone Daily L3 Global 1 Deg. CMG data set was acquired from the Level-1 and Atmosphere Archive & Distribution System (LAADS) Distributed Active Archive Center (DAAC), located in the Goddard Space Flight Center in Greenbelt, Maryland (https://ladsweb.nascom.nasa.gov/). We thank the PI investigators (Z. Li, B-B Chen, P. Goloub, J. Elizabeth Nichol, and L. Wu) and their staff for establishing and maintaining the four AERONET sites used in this investigation. The National Center for Atmospheric Research (NCAR) is sponsored by the National Science Foundation (NSF). We thank the EDGAR HTAP team for providing HTAP_V2 emissions inventory data (http://edgar.jrc.ec.europa.eu/htap_v2/). The authors acknowledge high-performance computing support from Cheyenne (doi:10.5065/D6RX99HX), provided by NCAR's Computational and Information Systems Laboratory, sponsored by the NSF. The Weather Research and Forecasting model is a free-to-use community model (https://ruc.noaa.gov/wrf/wrf-chem/). Code developments to carry out double radiation were released to the community in WRF-Chem version 4.0. We acknowledge use of the WRF-Chem preprocessor tools mozbc, fire_emiss, anthro_emiss, and bio_emiss, available from the Atmospheric Chemistry Observations & Modeling website (https://www2.acom.ucar.edu/wrf-chem/wrf-chem-tools-community). Figures and analysis were conducted using the NCAR Command Language (NCL) version 6.3.0 and the Anaconda distribution of Python version 3.6. Code for carrying out analysis of double calls for radiative forcing calculations from WRF-Chem model output is hosted on a github repository by D. Lowe (https://github.com/douglowe/WRFChem-ARC-Interactions). Processed monthly averaged WRF-Chem model data used for most of the analysis is available for download from ftp://ftp.acom.ucar.edu/user/nicholls. Due to its size the raw hourly 3D model output files are only available on request. Any opinions, findings, and conclusions expressed in the publication are those of the authors and do not necessarily reflect the views of the NSF or EPA. Finally, we thank the three anonymous reviewers for their positive, helpful, and insightful comments, which have greatly improved the paper.

References

Abdul-razzak, H., & Ghan, S. J. (2002). A parameterization of aerosol activation 3. Sectional representation. *Journal of Geophysical Research*, *107*(D3), 4026. https://doi.org/10.1029/2001JD000483

Akagi, S. K., Yokelson, R. J., Wiedinmyer, C., Alvarado, M. J., Reid, J. S., Karl, T., et al. (2011). Emission factors for open and domestic biomass burning for use in atmospheric models. *Atmospheric Chemistry and Physics*, *11*(9), 4039–4072. https://doi.org/10.5194/acp-11-4039-2011

Allen, R. J., & Sherwood, S. C. (2010). Aerosol-cloud semi-direct effect and land-sea temperature contrast in a GCM. *Geophysical Research Letters*, *37*, L07702. https://doi.org/10.1029/2010GL042759

Andreae, M. O., & Gelencs, A. (2006). Black carbon or brown carbon? The nature of light-absorbing carbonaceous aerosols. *Atmospheric Chemistry and Physics*, *6*, 3131–3148.

Andrews, E., Ogren, J. A., Kinne, S., & Samset, B. (2017). Comparison of AOD, AAOD and column single scattering albedo from AERONET retrievals and in situ profiling measurements. *Atmospheric Chemistry and Physics*, *17*, 6041–6072. https://doi.org/10.5194/acp-17-6041-2017

Anenberg, S. C., Schwartz, J., Shindell, D., Amann, M., Faluvegi, G., Klimont, Z., et al. (2012). Global air quality and health co-benefits of mitigating near-term climate change through methane and black carbon emission controls. *Environmental Health Perspectives*, *120*(6), 831–839. https://doi.org/10.1289/ehp.1104301

Archer-Nicholls, S., Carter, E., Kumar, R., Xiao, Q., Frostad, J., Forouzanfar, M. H., et al. (2016). The regional impact of cooking and heating emissions on air quality and disease burden in China. *Environmental Science & Technology*, *50*(17), 9416–9423. https://doi.org/10.1021/acs.est.6b02533

Archer-Nicholls, S., Lowe, D., Schultz, D. M., & Mcfiggans, G. (2016). Aerosol-radiation-cloud interactions in a regional coupled model: The effects of convective parameterisation and resolution. *Atmospheric Chemistry and Physics*, *16*, 5573–5594. https://doi.org/10.5194/acp-16-5573-2016

Aunan, K., Berntsen, T. K., Myhre, G., Rypdal, K., Streets, D. G., Woo, J. H., & Smith, K. R. (2009). Radiative forcing from household fuel burning in Asia. *Atmospheric Environment*, *43*(35), 5674–5681. https://doi.org/10.1016/j.atmosenv.2009.07.053

Bailis, R., Drigo, R., Ghilardi, A., & Masera, O. (2015). The carbon footprint of traditional woodfuels. *Nature Climate Change*, *5*, 266–272. https://doi.org/10.1038/nclimate2491

Barnard, J. C., Fast, J. D., Paredes-Miranda, G., Arnott, W. P., & Laskin, A. (2010). Technical note: Evaluation of the WRF-Chem "Aerosol Chemical to Aerosol Optical Properties" module using data from the MILAGRO campaign. *Atmospheric Chemistry and Physics*, *10*, 7325–7340. https://doi.org/10.5194/acp-10-7325-2010

Bohren, C. Z., & Huffman, D. R. (1983). Absorption and Scattering of Light by Small Particles. New York, USA: Wiley.

Bond, T. C., Bhardwaj, E., Dong, R., Jogani, R., Jung, S., Roden, C., et al. (2007). Historical emissions of black and organic carbon aerosol from energy-related combustion, 1850–2000. *Global Biogeochemical Cycles*, *21*, GB2018. https://doi.org/10.1029/2006GB002840

Bond, T. C., Doherty, S. J., Fahey, D. W., Forster, P. M., Berntsen, T., Deangelo, B. J., et al. (2013). Bounding the role of black carbon in the climate system: A scientific assessment. *Journal of Geophysical Research: Atmospheres*, *11*, 5380–5552. https://doi.org/10.1002/jgrd.50171

Bond, T. C., Habib, G., & Bergstrom, R. W. (2006). Limitations in the enhancement of visible light absorption due to mixing state. *Journal of Geophysical Research*, *111*, D20211. https://doi.org/10.1029/2006JD007315

Boucher, O., Randall, D., Artaxo, P., Bretherton, C., Feingold, G., Forster, P., et al. (2013). Clouds and Aerosols. In T. F. Stocker, et al. (Eds.), *Climate change 2013: The physical science basis. Contribution of Working Group I to the Fifth Assessment Report of the Intergovernmental Panel on Climate Change*. Cambridge, United Kingdom and New York, NY, USA: Cambridge University Press.

Butt, E. W., Rap, A., Schmidt, A., Scott, C. E., Pringle, K. J., Reddington, C. L., et al. (2016). The impact of residential combustion emissions on atmospheric aerosol, human health and climate. *Atmospheric Chemistry and Physics*, *15*(14), 20,449–20,520. https://doi.org/10.5194/acpd-15-20449-2015

Carter, E. M., Archer-Nicholls, S., Ni, K., Lai, A. M., Niu, H., Secrest, M. H., et al. (2016). Seasonal and diurnal air pollution from residential cooking and space heating in the Eastern Tibetan Plateau. *Environmental Science & Technology*, *50*(15), 8353–8361. https://doi.org/10.1021/acs.est.6b00082

Chafe, Z. A., Brauer, M., Klimont, Z., Van Dingenen, R., Mehta, S., Rao, S., et al. (2014). Household cooking with solid fuels contributes to ambient PM 2.5 air pollution and the burden of disease. *Environmental Health Perspectives*, *122*(12), 1314–1320. https://doi.org/10.1289/ehp.1206340

Chapman, E. G., Gustafson, W. I. Jr., Easter, R. C., Barnard, J. C., Ghan, S. J., Pekour, M. S., & Fast, J. D. (2009). Coupling aerosol-cloud-radiative processes in the WRF-Chem model: Investigating the radiative impact of elevated point sources. *Atmospheric Chemistry and Physics*, *9*, 945–964.

Chen, D., Liu, Z., Fast, J., & Ban, J. (2016). Simulations of sulfate-nitrate-ammonium (SNA) aerosols during the extreme haze events over Northern China in October 2014. *Atmospheric Chemistry and Physics*, *16*, 10,707–10,724. https://doi.org/10.5194/acp-2016-222

Chen, S., Zhao, C., Qian, Y., Leung, L. R., Huang, J., Huang, Z., et al. (2014). Regional modeling of dust mass balance and radiative forcing over East Asia using WRF-Chem. *Aeolian Research*, *15*, 15–30. https://doi.org/10.1016/j.aeolia.2014.02.001

Chen, S. R., Xu, L., Zhang, Y. X., Chen, B., Wang, X. F., Zhang, X. Y., et al. (2017). Direct observations of organic aerosols in common wintertime hazes in North China: Insights into direct emissions from Chinese residential stoves. *Atmospheric Chemistry and Physics*, *17*, 1–32. https://doi.org/10.5194/acp-2016-494

Coffey, E. R., Muvandimwe, D., Hagar, Y., Wiedinmyer, C., Kanyomse, E., Piedrahita, R., et al. (2017). New emission factors and efficiencies from in-field measurements of traditional and improved cookstoves and their potential implications. *Environmental Science & Technology*, *51*(21), 12,508–12,517. https://doi.org/10.1021/acs.est.7b02436

Cohen, A. J., Brauer, M., Burnett, R., Anderson, H. R., Frostad, J., Estep, K., et al. (2017). Estimates and 25-year trends of the global burden of disease attributable to ambient air pollution: An analysis of data from the Global Burden of Diseases Study 2015. *The Lancet*, *389*(10082), 1907–1918. https://doi.org/10.1016/S0140-6736(17)30505-6

Emmons, L. K., Walters, S., Hess, P. G., Lamarque, J.-F., Pfister, G. G., Fillmore, D., et al. (2010). Description and evaluation of the Model for Ozone and Related chemical Tracers, version 4 (MOZART-4). *Geoscientific Model Development*, *3*(1), 43–67. https://doi.org/10.5194/gmd-3-43-2010

Fast, J. D., Gustafson, W. I., Easter, R. C., Zaveri, R. A., Barnard, J. C., Chapman, E. G., et al. (2006). Evolution of ozone, particulates, and aerosol direct radiative forcing in the vicinity of Houston using a fully coupled meteorology-chemistry-aerosol model. *Journal of Geophysical Research*, *111*, D21305. https://doi.org/10.1029/2005JD006721

Gao, M., Carmichael, G. R., Wang, Y., Saide, P. E., Yu, M., Xin, J., et al. (2016). Modeling study of the 2010 regional haze event in the North China Plain. *Atmospheric Chemistry and Physics*, *15*(16), 22,781–22,822. https://doi.org/10.5194/acpd-15-22781-2015

Gao, M., Ji, D., Liang, F., & Liu, Y. (2018). Attribution of aerosol direct radiative forcing in China and India to emitting sectors. *Atmospheric Environment*, *190*(June), 35–42. https://doi.org/10.1016/j.atmosenv.2018.07.011

Gao, M., Saide, P. E., Xin, J., Wang, Y., Liu, Z., Wang, Y., et al. (2017). Estimates of health impacts and radiative forcing in winter haze in Eastern China through constraints of surface PM2.5 predictions. *Environmental Science and Technology*, *51*(4), 2178–2185. https://doi.org/10.1021/acs.est.6b03745

Ghan, S. J., Liu, X., Easter, R. C., Zaveri, R., Rasch, P. J., Yoon, J.-H., & Eaton, B. (2012). Toward a minimal representation of aerosols in climate models: Comparative decomposition of aerosol direct, semidirect, and indirect radiative forcing. *Journal of Climate*, *25*, 6461–6476. https://doi.org/10.1175/JCLI-D-11-00650.1

Grell, G., Freitas, S. R., Stuefer, M., & Fast, J. (2011). Inclusion of biomass burning in WRF-Chem: Impact of wildfires on weather forecasts. *Atmospheric Chemistry and Physics*, *11*(11), 5289–5303. https://doi.org/10.5194/acp-11-5289-2011

Grell, G. A., & Devenyi, D. (2002). A generalized approach to parameterizing convection combining ensemble and data assimilation techniques. *Geophysical Research Letters*, *29*(14), 1693. https://doi.org/10.1029/2002GL015311

Grell, G. A., & Freitas, S. R. (2014). A scale and aerosol aware stochastic convective parameterization for weather and air quality modeling. *Atmospheric Chemistry and Physics*, *14*, 5233–5250. https://doi.org/10.5194/acp-14-5233-2014

Grell, G. A., Peckham, S. E., Schmitz, R., McKeen, S. A., Frost, G., Skamarock, W. C., & Eder, B. (2005). Fully coupled "online" chemistry within the WRF model. *Atmospheric Environment*, *39*(37), 6957–6975. https://doi.org/10.1016/j.atmosenv.2005.04.027

Guenther, A. B., Jiang, X., Heald, C. L., Sakulyanontvittaya, T., Duhl, T., Emmons, L. K., & Wang, X. (2012). The model of emissions of gases and aerosols from nature version 2.1 (MEGAN2.1): An extended and updated framework for modeling biogenic emissions. *Geoscientific Model Development*, *5*, 1471–1492. https://doi.org/10.5194/gmd-5-1471-2012

Haywood, J., & Boucher, O. (2000). Estimates of the direct and indirect radiative forcing due to tropospheric aerosols: A review. *Reviews of Geophysics*, *38*(4), 513. https://doi.org/10.1029/1999RG000078

Haywood, J. M., & Shine, K. P. (1995). The effect of anthropogenic sulfate and soot aerosol on the clear sky planetary radiation budget. *Geophysical Research Letters*, *22*(5), 603–606.

Holben, B. N., Eck, T. F., Slutsker, I., Tanre, D., Buis, J. P., Setzer, A., et al. (1998). AERONET—A federated instrument network and data archive for aerosol characterization. *Remote Sensing of Environment*, *66*(1), 1–16. https://doi.org/10.1016/S0034-4257(98)00031-5

Holben, N., Tanr, D., Smirnov, A., Eck, T. F., Slutsker, I., Newcomb, W. W., et al. (2001). An emerging ground-based aerosol climatology: Aerosol optical depth from AERONET. *Journal of Geophysical Research*, *106*(D11), 12,067–12,097. https://doi.org/10.1029/2001JD900014

Huang, X., Song, Y., Zhao, C., Cai, X., Zhang, H., & Zhu, T. (2015). Direct radiative effect by multicomponent aerosol over China. *Journal of Climate*, *28*(9), 3472–3495. https://doi.org/10.1175/JCLI-D-14-00365.1

Iacono, M. J., Mlawer, E. J., & Clough, S. A. (2000). Impact of an improved longwave radiation model, RRTM, on the energy budget and thermodynamic properties of the NCAR community climate model, CCM3. *Journal of Geophysical Research*, *105*(D11), 14,873–14,890.

Jackson, S. C. (2009). Parallel pursuit of near-term and long-term climate mitigation. *Science*, *326*(5952), 526–527. https://doi.org/10.1126/science.1177042

Janssens-Maenhout, G., Crippa, M., Guizzardi, D., Dentener, F., Muntean, M., Pouliot, G., et al. (2015). HTAP_v2.2: A mosaic of regional and global emission grid maps for 2008 and 2010 to study hemispheric transport of air pollution. *Atmospheric Chemistry and Physics*, *15*(19), 11,411–11,432. https://doi.org/10.5194/acp-15-11411-2015

Janssens-Maenhout, G., Dentener, F., Van Aardenne, J., Monni, S., Pagliari, V., Orlandini, L., et al. (2012). EDGAR-HTAP: A harmonized gridded air pollution emission dataset based on national inventories. EUR 25229 EN Report. https://doi.org/10.2788/14102

Klimont, Z., Kupianinen, K., Heyes, C., Purohit, P., Cofala, J., Rafaj, P., et al. (2017). Global anthropogenic emissions of particulate matter including black carbon. *Atmospheric Chemistry and Physics*, *17*(14), 8681–8723. https://doi.org/10.5194/acp-17-8681-2017

Knote, C., Hodzic, A., & Jimenez, J. L. (2015). The effect of dry and wet deposition of condensable vapors on secondary organic aerosols concentrations over the continental US. *Atmospheric Chemistry and Physics*, *15*, 1–18. https://doi.org/10.5194/acpd-14-13731-2014

Knote, C., Hodzic, a., Jimenez, J. L., Volkamer, R., Orlando, J. J., Baidar, S., et al. (2014). Simulation of semi-explicit mechanisms of SOA formation from glyoxal in aerosol in a 3-D model. *Atmospheric Chemistry and Physics*, *14*(12), 6213–6239. https://doi.org/10.5194/acp-14-6213-2014

Koch, D., & Del Genio, A. D. (2010). Black carbon semi-direct effects on cloud cover: review and synthesis. *Atmospheric Chemistry and Physics*, *10*, 7685–7696. https://doi.org/10.5194/acp-10-7685-2010

Kodros, J. K., Hanna, S., Bertram, A., Leaitch, W. R., Schulz, H., Zanatta, M., et al. (2018). Size-resolved mixing state of black carbon in the Canadian high Arctic and implications for simulated direct radiative effect. *Atmospheric Chemistry and Physics*, *18*(15), 11,345–11,361. https://doi.org/10.5194/acp-18-11345-2018

Kodros, J. K., Scott, C. E., Farina, S. C., Lee, Y. H., Orange, C. L., Volckens, J., & Pierce, J. R. (2015). Uncertainties in global aerosols and climate effects due to biofuel emissions. *Atmospheric Chemistry and Physics Discussions*, *15*, 10,199–10,256. https://doi.org/10.5194/acpd-15-10199-2015

Lacey, F., & Henze, D. (2015). Global climate impacts of country-level primary carbonaceous aerosol from solid-fuel cookstove emissions. *Environmental Research Letters*, *10*(11), 114003. https://doi.org/10.1088/1748-9326/10/11/114003

Lack, D. A., Langridge, J. M., Bahreini, R., Cappa, C. D., Middlebrook, A. M., & Schwarz, J. P. (2012). Brown carbon and internal mixing in biomass burning particles. *Proceedings of the National Academy of Sciences of the United States of America*, *109*(37), 14,802–14,807. https://doi.org/10.1073/pnas.1206575109

Lau, W. K. M., Sang, J., Kim, M. K., Kim, K. M., Koster, R. D., & Yasunari, T. J. (2018). Impacts of aerosol snow darkening effects on hydro-climate over Eurasia during boreal spring and summer. *Journal of Geophysical Research: Atmospheres*, *123*, 8441–8461. https://doi.org/10.1029/2018JD028557

Lee, L. A., Reddington, C. L., & Carslaw, K. S. (2016). On the relationship between aerosol model uncertainty and radiative forcing uncertainty. *Proceedings of the National Academy of Sciences*, *113*(21), 5820–5827. https://doi.org/10.1073/pnas.1507050113

Lelieveld, J., Evans, J. S., Fnais, M., Giannadaki, D., & Pozzer, A. (2015). The contribution of outdoor air pollution sources to premature mortality on a global scale. *Nature*, *525*(7569), 367–371. https://doi.org/10.1038/nature15371

Li, H., Zhang, Q., Zheng, B., Chen, C., Wu, N., Guo, H., et al. (2018). Nitrate-driven urban haze pollution during summertime over the North China Plain. *Atmospheric Chemistry and Physics*, *18*(8), 5293–5306. https://doi.org/10.5194/acp-18-5293-2018

Li, J., Bo, Y., & Xie, S. (2016). Estimating emissions from crop residue open burning in China based on statistics and MODIS fire products. *Journal of Environmental Sciences (China)*, *44*, 158–170. https://doi.org/10.1016/j.jes.2015.08.024

Li, K., Liao, H., Mao, Y., & Ridley, D. A. (2015). Source sector and region contributions to concentration and direct radiative forcing of black carbon in China. *Atmospheric Environment*. https://doi.org/10.1016/j.atmosenv.2015.06.014

Li, M., Zhang, Q., Kurokawa, J., Woo, J., He, K., Lu, Z., & Ohara, T. (2017). MIX: A mosaic Asian anthropogenic emission inventory under the international collaboration framework of the MICS-Asia and HTAP. *Atmospheric Chemistry and Physics*, *17*, 935–963. https://doi.org/10.5194/acp-17-935-2017

Liu, J., Mauzerall, D. L., Chen, Q., Zhang, Q., Song, Y., Peng, W., et al. (2016). Air pollutant emissions from Chinese households: A major and underappreciated ambient pollution source. *Proceedings of the National Academy of Sciences*, *113*(28), 7756–7761. https://doi.org/10.1073/pnas.1604537113

Lohmann, U., & Feichter, J. (2005). Global indirect aerosol effects: A review. *Atmospheric Chemistry and Physics*, *5*, 715–737.

Matsui, H., Hamilton, D. S., & Mahowald, N. M. (2018). Black carbon radiative effects highly sensitive to emitted particle size when resolving mixing-state diversity. *Nature Communications*, *9*(1), 3446. https://doi.org/10.1038/s41467-018-05635-1

Matsui, H., Koike, M., Kondo, Y., Moteki, N., Fast, J. D., & Zaveri, R. A. (2013). Development and validation of a black carbon mixing state resolved three-dimensional model: Aging processes and radiative impact. *Journal of Geophysical Research: Atmospheres*, *118*, 2304–2326. https://doi.org/10.1029/2012JD018446

Myhre, G., Shindell, D., Bréon, F.-M., Collins, W., Fuglestvedt, J., Huang, J., et al. (2013). Anthropogenic and Natural Radiative Forcing. In *Climate change 2013: The physical science basis. Contribution of Working Group I to the Fifth Assessment Report of the Intergovernmental Panel on Climate Change* (pp. 659–740). United Kingdom and New York, NY, USA: Cambridge University Press.

Naeher, L. P., Brauer, M., Lipsett, M., Zelikoff, J. T., Simpson, C. D., Koenig, J. Q., & Smith, K. R. (2007). Woodsmoke health effects: A review. *Inhalation Toxicology*, *19*, 67–106. https://doi.org/10.1080/08958370600985875

Olivier, J. G. J., Peters, J., Granier, C., Petron, G., Muller, J.-F., & Wallens, S. (2003). Present and future surface emissions of atmospheric compounds. *POET Report #3, EU Project EVK2–1999-00011*.

Ramanathan, V., & Carmichael, G. (2008). Global and regional climate changes due to black carbon. *Nature Geoscience*, *1*(4), 221–227. https://doi.org/10.1038/ngeo156

Ramanathan, V., Crutzen, P. J., Kiehl, J. T., & Rosenfeld, D. (2001). Aerosols, climate, and the hydrological cycle. *Science (New York, N.Y.)*, *294*(2119), 2119–2124. https://doi.org/10.1126/science.1064034

Remer, L. A., Kaufman, Y. J., Tanré, D., Mattoo, S., Chu, D. A., Martins, J. V., et al. (2005). The MODIS aerosol algorithm, products, and validation. *Journal of the Atmospheric Sciences*, *62*(4), 947–973. https://doi.org/10.1175/JAS3385.1

Rohde, R. A., & Muller, R. A. (2015). Air pollution in China: Mapping of concentrations and sources. *PLoS ONE*, *10*(8), 1–14. https://doi.org/10.1371/journal.pone.0135749

Saide, P. E., Spak, S. N., Carmichael, G. R., Mena-Carrasco, M. A., Yang, Q., Howell, S., et al. (2012). Evaluating WRF-chem aerosol indirect effects in southeast pacific marine stratocumulus during VOCALS-REx. *Atmospheric Chemistry and Physics*, *12*(6), 3045–3064. https://doi.org/10.5194/acp-12-3045-2012

Secrest, M. H., Schauer, J. J., Carter, E. M., & Baumgartner, J. (2017). Particulate matter chemical component concentrations and sources in settings of household solid fuel use. *Indoor Air*, *27*(6), 1052–1066. https://doi.org/10.1111/ina.12389

Shindell, D., Kuylenstierna, J. C. I., Vignati, E., van Dingenen, R., Amann, M., Klimont, Z., et al. (2012). Simultaneously mitigating near-term climate change and improving human health and food security. *Science*, *335*(6065), 183–189. https://doi.org/10.1126/science.1210026

Stjern, C. W., Samset, B. H., Myhre, G., Forster, P. M., Hodnebrog, Ø., Andrews, T., et al. (2017). Rapid adjustments cause weak surface temperature response to increased black carbon concentrations. *Journal of Geophysical Research: Atmospheres*, *122*, 11,462–11,481. https://doi.org/10.1002/2017JD027326

Stockwell, C. E., Veres, P. R., Williams, J., & Yokelson, R. J. (2015). Characterization of biomass burning smoke from cooking fires, peat, crop residue and other fuels with high resolution proton-transfer-reaction time-of-flight mass spectrometry. *Atmospheric Chemistry and Physics*, *15*, 845–865. https://doi.org/10.5194/acp-15-845-2015

Streets, D. G., Bond, T. C., Carmichael, G. R., Fernandes, S. D., Fu, Q., He, D., et al. (2003). An inventory of gaseous and primary aerosol emissions in Asia in the year 2000. *Journal of Geophysical Research*, *108*(D21), 8809. https://doi.org/10.1029/2002JD003093

Sun, J., Zhi, G., Hitzenberger, R., Chen, Y., Tian, C., Zhang, Y., et al. (2017). Emission factors and light absorption properties of brown carbon from household coal combustion in China. *Atmospheric Chemistry and Physics*, *17*(7), 4769–4780. https://doi.org/10.5194/acp-17-4769-2017

Turpin, B. J., & Lim, H. (2001). Species contributions to PM2. 5 mass concentrations: Revisiting common assumptions for estimating organic mass. *Aerosol Science and Technology*, *35*, 602–610.

Unger, N., Bond, T. C., Wang, J. S., Koch, D. M., Menon, S., Shindell, D. T., & Bauer, S. (2010). Attribution of climate forcing to economic sectors. *Proceedings of the National Academy of Sciences*, *107*(8), 3382–3387. https://doi.org/10.1073/pnas.0906548107

Wang, X., Liang, X. Z., Jiang, W., Tao, Z., Wang, J. X. L., Liu, H., et al. (2010). WRF-Chem simulation of East Asian air quality: Sensitivity to temporal and vertical emissions distributions. *Atmospheric Environment*, *44*(5), 660–669. https://doi.org/10.1016/j.atmosenv.2009.11.011

Wiedinmyer, C., Akagi, S. K., Yokelson, R. J., Emmons, L. K., Al-Saadi, J. A., Orlando, J. J., & Soja, A. J. (2011). The Fire INventory from NCAR (FINN): A high resolution global model to estimate the emissions from open burning. *Geoscientific Model Development*, *4*, 625–641. https://doi.org/10.5194/gmd-4-625-2011

Yang, Q., Fast, J. D., Wang, H., Easter, R. C., Morrison, H., Lee, Y.-N., et al. (2011). Assessing regional scale predictions of aerosols, marine stratocumulus, and their interactions during VOCALS-REx using WRF-Chem. *Atmospheric Chemistry and Physics*, *11*(23), 11,951–11,975. https://doi.org/10.5194/acp-11-11951-2011

Yang, Y., Smith, S. J., Wang, H., Mills, C. M., & Rasch, P. J. (2019). Variability, timescales, and non-linearity in climate responses to black carbon emissions. *Atmospheric Chemistry and Physics*, *19*, 2405–2420. https://doi.org/10.5194/acp-2018-904

Yao, H., Song, Y., Liu, M., Archer-Nicholls, S., Lowe, D., McFiggans, G., et al. (2017). Direct radiative effect of carbonaceous aerosols from crop residue burning during the summer harvest season in East China. *Atmospheric Chemistry and Physics*, *17*(8), 5205–5219. https://doi.org/10.5194/acp-17-5205-2017

Yu, S., Eder, B., Dennis, R., Chu, S.-H., & Schwartz, S. E. (2006). New unbiased symmetric metrics for evaluation of air quality models. *Atmospheric Science Letters*, *7*(1), 26–34. https://doi.org/10.1002/asl.125

Zaveri, R. A., Easter, R. C., Fast, J. D., & Peters, L. K. (2008). Model for simulating aerosol interactions and chemistry (MOSAIC). *Journal of Geophysical Research*, *113*, D13204. https://doi.org/10.1029/2007JD008782

Zhang, Q., Streets, D. G., Carmichael, G. R., He, K. B., Huo, H., Kannari, A., et al. (2009). Asian emissions in 2006 for the NASA INTEX-B mission. *Atmospheric Chemistry and Physics*, *9*(14), 5131–5153. https://doi.org/10.5194/acp-9-5131-2009

Zhang, Q., Streets, D. G., He, K., & Klimont, Z. (2007). Major components of China's anthropogenic primary particulate emissions. *Environmental Research Letters*, *2*(4). https://doi.org/10.1088/1748-9326/2/4/045027

Zhang, R., Wang, G., Guo, S., Zamora, M. L., Ying, Q., Lin, Y., et al. (2015). Formation of Urban Fine Particulate Matter. *Chemical Reviews*, *115*(10), 3803–3855. https://doi.org/10.1021/acs.chemrev.5b00067

Zhang, W., Lu, Z., Xu, Y., Wang, C., Gu, Y., Xu, H., & Streets, D. G. (2018). Black carbon emissions from biomass and coal in rural China. *Atmospheric Environment*, *176*, 158–170. https://doi.org/10.1016/j.atmosenv.2017.12.029

Zheng, G. J., Duan, F. K., Su, H., Ma, Y. L., Cheng, Y., Zheng, B., et al. (2015). Exploring the severe winter haze in Beijing: The impact of synoptic weather, regional transport and heterogeneous reactions. *Atmospheric Chemistry and Physics*, *15*(6), 2969–2983. https://doi.org/10.5194/acp-15-2969-2015

Zheng, B., Tong, D., Li, M., Liu, F., Hong, C., Geng, G., et al. (2018). Trends in China's anthropogenic emissions since 2010 as the consequence of clean air actions. *Atmospheric Chemistry and Physics*, *18*(19), 14,095–14,111. https://doi.org/10.5194/acp-18-14095-2018